NTNU

Norwegian University of
Science and Technology

Three-dimensional wake measurements

Pål Egil Eriksen

Master of Science in Energy and Environment
Submission date: June 2010
Supervisor: Per-Åge Krogstad, EPT

Norwegian University of Science and Technology
Department of Energy and Process Engineering

Problem Description

Objective

The student should perform measurements in the wake of a stationary body with cyclic vortex shedding (e.g. the wake behind a cylinder) to study such flow fields. The student is free to choose a suitable measurement technique for this purpose, the measurement technique chosen must however have both excellent spatial and temporal resolution.

The following questions should be considered in the project work:

1. The student shall investigate the performance of a suitable measurement technique for three-dimensional unsteady flows such as e.g. three component hot wire anemometry
2. If the method is deemed suitable, he should perform measurements in the wake of a blunt body to see if the periodic flow may be picked up by the measurement technique.

Assignment given: 18. January 2010
Supervisor: Per-Åge Krogstad, EPT

NTNU
Norwegian University
of Science and Technology

Department of Energy
and Process Engineering

EPT-M-2010-15

MASTER THESIS

for

Stud.techn. Pål Egil Eriksen
Spring 2010

Three-dimensional wake measurements

Tredimensjonale wake målinger

Background

The performance of a wind turbine is often found using a blade element momentum method, which assumes the flow field to be uniform and without turbulent motions. It is obvious that a turbine operating in the wake behind one or more wind turbines will experience a very different flow field. Measurements done in wind tunnels, in our laboratory as well as others, show the phase averaged velocity field in such a wake to be complex and highly dependent on the state of operation of the upstream turbine(s). The instantaneous flow field of such a wake will be even more complicated, showing a statistically random pattern of turbulent motions. Some degree of order can however be found as the flow field is repeated by each passage of the turbine blades. To perform measurements of the full time-dependent velocity vector in such a geometry is a difficult task and as a preparatory investigation it is desirable to investigate the performance of a suitable measurement technique in a similar, but not as complicated flow, such as can be found behind a stationary body.

Objective

The student should perform measurements in the wake of a stationary body with cyclic vortex shedding (e.g. the wake behind a cylinder) to study such flow fields. The student is free to choose a suitable measurement technique for this purpose, the measurement technique chosen must however have both excellent spatial and temporal resolution.

The following questions should be considered in the project work:

1. The student shall investigate the performance of a suitable measurement technique for three-dimensional unsteady flows such as e.g. three component hot wire anemometry
2. If the method is deemed suitable, he should perform measurements in the wake of a blunt body to see if the periodic flow may be picked up by the measurement technique.

-- " --

Within 14 days of receiving the written text on the diploma thesis, the candidate shall submit a research plan for his project to the department.

When the thesis is evaluated, emphasis is put on processing of the results, and that they are presented in tabular and/or graphic form in a clear manner, and that they are analyzed carefully.

The thesis should be formulated as a research report with summary both in English and Norwegian, conclusion, literature references, table of contents etc. During the preparation of the text, the candidate should make an effort to produce a well-structured and easily readable reportreport. In order to ease the evaluation of the thesis, it is important that the cross-references are correct. In the making of the report, strong emphasis should be placed on both a thorough discussion of the results and an orderly presentation.

The candidate is requested to initiate and keep close contact with his/her academic supervisor(s) throughout the working period. The candidate must follow the rules and regulations of NTNU as well as passive directions given by the Department of Energy and Process Engineering.

Pursuant to "Regulations concerning the supplementary provisions to the technology study program/Master of Science" at NTNU §20, the Department reserves the permission to utilize all the results and data for teaching and research purposes as well as in future publications.

One – 1 complete original of the thesis shall be submitted to the authority that handed out the set subject. (A short summary including the author's name and the title of the thesis should also be submitted, for use as reference in journals (max. 1 page with double spacing)).
Two – 2 – copies of the thesis shall be submitted to the Department. Upon request, additional copies shall be submitted directly to research advisors/companies. A CD-ROM (Word format or corresponding) containing the thesis, and including the short summary, must also be submitted to the Department of Energy and Process Engineering

Department of Energy and Process Engineering, 12. January 2010

Olav Bolland
Department Head

Per-Åge Krogstad
Academic Supervisor

Research Advisors:

Acknowledgments

This Masterthesis is completed at the Department of Applied Mechanics, Thermo- and Fluid Dynamics at the Norwegian University of Science and Technology.

I am most grateful to my supervisor Professor Per-Åge Krogstad for his guidance and encouragement in the process of completing this thesis. His insight and constructive advise has been of good help.

Trondheim, 14 juni 2010

Pål Egil Eriksen

Abstract

The performance of a hot wire probe with three wires is investigated for two different flow cases. The wires are made of a platinum/rhodium alloy, and has a diameter of $5\mu m$. The three wires make a probe volume with a cross section of approximately 5 mm. A cosinus fit using the effective angle method gives a deviation of $\pm 1^\circ$ for a variation of yaw angle equal to $\pm 20^\circ$. First the probe was tested in a fully developed turbulent pipe flow, for $\Re_D = 10^5$. Good results were obtained for $|y/R| < 0.8$, both for mean velocities and turbulent stresses. Closer to the wall the mean flow gradient was too large relative to the probe resolution, giving large errors. The second flow case was a cylinder wake. A traverse of the flow at $x/D = 10$ was performed at $\Re_D = 3 \cdot 10^3$. The mean velocities and turbulent stresses was partly found to be in qualitative agreement with results found in litterature. The shear stresses $\overline{uw}$ and $\overline{vw}$ were however found to be unphysically large, this is believed to be due to the velocity gradient in the wake. Conditional averaging of the wake results with respect to shedding frequency was also conducted.

Sammendrag

Egenskapene til en hot wire probe med tre tråder har blitt undersøkt for to forskjellige strømnings tilfeller. Trådene er laget av en platinum/rhodium legering og har en diameter på $5\mu m$. De tre trådene skaper eit probe volum med eit tverrsnitt på ca 5 mm. Effektiv vinkel metoden har blitt brukt og en tilpassning til en cosinus funksjon gir et avik på $\pm 1^\circ$ for en variasjon av yaw-vinkelen på $\pm 20^\circ$. Først ble proben testet i en fullt utviklet rørstrømning, med $\Re_D = 10^5$. Resultatene er i godt samsvar med teori og litteratur for $|y/R| < 0.8$, både mhp middelhastigeter og turbulente spenninger. Nær veggen ble gradienten til middelhastigheten stor i forhold til probens rommelige oppløsning, noe som ga store feil. Den andre strømningen som ble undersøkt var vaken bak ein sylinder for $\Re_D = 3 \cdot 10^3$. De målte middelhastighetene og turbulente spenningene var delvis i overenstemmelse med resultater fra litteratur. Skjærspenningene $\overline{uw}$ og $\overline{vw}$ var ufysisk store. Det antas at dette er på grunn av den store hastighetsgradienten i vaken. Midling med hensyn på virvelavløsnings frekvensen er og forsøkt.

Contents

1 Introduction

In complex flows it can be difficult to obtain good velocity measurements. Many measurement techniques depend on knowledge of the flow direction and is of limited value if it is unknown or varying with time. The wake behind a wind turbine is such a flow where the exact flow direction is both unknown and time varying. To perform successful single-point measurements in such a flow, a probe capable of measuring the velocity in all three dimensions is needed.

If the turbulent characteristics of the flow is of interest the temporal resolution must be good. The number of three dimensional measurement techniques with good temporal resolution is limited. 3D laser doppler anemometry is one option, hot wire probes with three or more wires is another. Both have their strengths and weaknesses.

In this project 3-wire constant temperature hot wire anemometry is studied. The goal is to learn if three component hot wire can be used in a complex and time varying flow to measure the mean velocities and turbulent stresses. To test the performance of the probe two different flow cases is examined. The first case is turbulent pipe flow. For this classic flow case, the measurements can be compared with analytic results, and it is therefore suitable as an initial test. The second case is the near wake of a cylinder. The cylinder wake can be analyzed both with respect to the mean flow and as a time varying flow where vortices are shed at a constant frequency from the cylinder. It is therefore suitable for assessing the capabilites of the probe in a dynamic flow.

2 Theory

This section explains the theory behind multi wire hot wire measurements and the basics of the flows that are investigated.

2.1 Theory of multi component hot wire measurements

The theory of single hot wire anemometry also applies to the individual wires of a 2 or 3 component hot wire. In this section the principles of multicomponent hot wire anemometry are investigated, knowledge of single hot wire anemometry is assumed to be a prerequisite.

2.1.1 Effective cooling velocity

Velocity measurements can be divided into two types. In many cases the flow direction is known or at least assumed to be known, the magnitude of the velocity is then of interest. In more complex flows the flow direction is unknown, and must be determined by measurements. A single hot wire can only determine the flow velocity V when the flow direction is known.

$$E^2 = A + BV^n \tag{1}$$

To also determine the flow direction, one needs a probe with at least one wire per dimension of interest. These wires are placed at angles to one another, and experience different magnitudes of cooling. A useful definition in this context is the effective cooling velocity defined by Jørgensen.

$$V_e{}^2 = U_n{}^2 + k^2 U_t{}^2 + h^2 U_b{}^2 \tag{2}$$

The effective cooling velocity is defined as the velocity normal to the wire which has the same cooling effect as the actual velocity vector. Equation 2 decomposes the effective cooling velocity into three components. Figure 1 shows how the different components are defined. U_n is the normal component, U_t is the tangential component and U_b is the binormal component which is normal to the n-t plane. The three components contribute unequally to the cooling of the wire. The coefficients k and h correct for the differences in cooling along the the different axes. K and h are not constants but functions of the flow direction given by α and β, the yaw and pitch angles, $k = k(\alpha)$ and $h = h(\beta)$. The tangential component is significantly less efficient at cooling the wire compared to the normal and binormal components. For an infinitely long wire, normal and binormal cooling should be equally effective. In the finite case the flow will be affected by the supporting prongs, but the effect is small and the normal and binormal velocity is often assumed to be equally effective, which implies that h can be set to 1.

2.1.2 The effective angle method

The effective cooling velocity can not be measured directly, but it can be estimated as a function of α. Consider first the two dimensional case, with no binormal

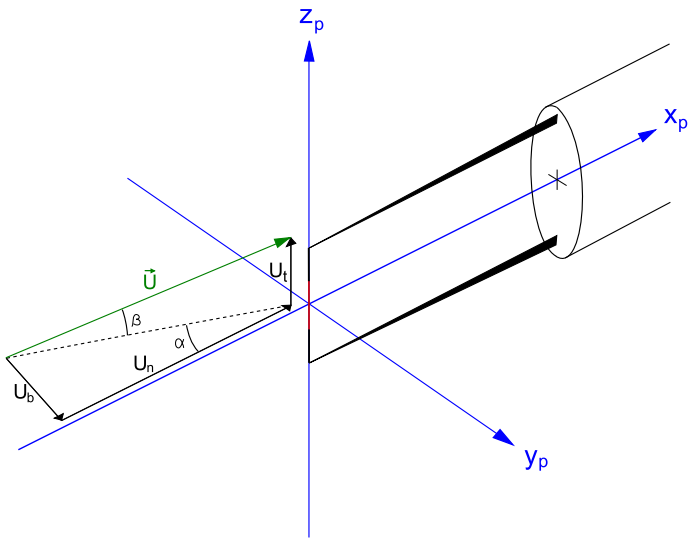

Figure 1: Definition of angles and cooling velocities relative to a single wire

cooling, as shown in figure 2(a). The effective cooling velocity can be related to the velocity vector S in the n-t plane by the function $f(\alpha)$. This the basis of the effective angle method, that the effective cooling velocity can be related to the flow velocity trough the yaw-angle α.

$$V_e = ({U_n}^2 + k^2 {U_t}^2)^{\frac{1}{2}} = Sf(\alpha) \tag{3}$$

F can be many different functions, but a cosine is a natural choice.

$$V_e = S\cos(\alpha_e + \alpha) \tag{4}$$

In equation 4 a new constant, α_e, is introduced. The wire in figure 2(b) is permanently yawed relative to the probe axis, y_p by the angle α_e. Equation 4 therefore gives us the component of the velocity vector S which is normal to the wire, as a function of α and α_e.

When a velocity calibration of the wire is conducted, the probe axis x_p is aligned with the flow direction, hence α is zero(see figure 2(a)). The measured voltage output, E, then corresponds to a given velocity, U, which is the same as the known velocity vector S. Equation 4 can for this case be written:

$$V_e = S\cos(\alpha_e) = U\cos(\alpha_e) \tag{5}$$

If the probe is yawed an angle α (see figure 2(b)), for the same velocity S, the voltage output E_{yawed} will correspond to a velocity U_{yawed} which is obtained from the velocity calibration. U_{yawed} is different from S. Two different expressions for the effective cooling velocity may now be written. Equation 6 gives the effective cooling velocity as the component of S which is normal to the wire.

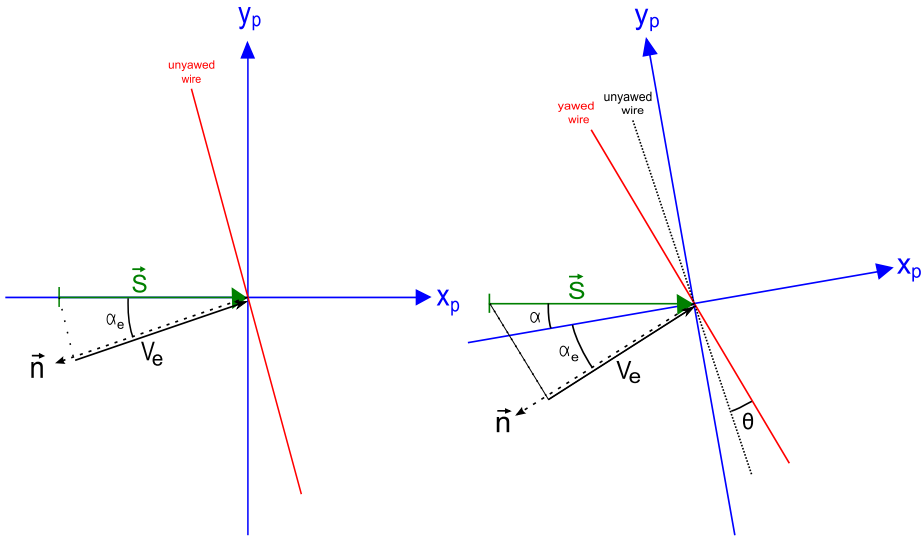

(a) Unyawed (b) Yawed

Figure 2: Velocity definitions in the normal-tangential plane

$$V_e = S\cos(\alpha_e + \alpha) \tag{6}$$

The effective cooling velocity can also be written as the component of U_{yawed} which is normal to the wire. This relation will not depend on α since U_{yawed} has a fixed flow direction relative to the probe.

$$V_e = U_{yawed}\cos(\alpha_e) \tag{7}$$

By combining equation 6 and 7 a relation between the true velocity vector S, the flow direction alpha and the velocity U_{yawed} is found. From now on we will denote U_{yawed} in the more general form U(E), referring to the fact that U is found from the hot wire voltage E through the velocity calibration.

$$V_e = S\cos(\alpha_e + \alpha) = U(E)\cos(\alpha_e) \tag{8}$$

In the case where S and α is unknown, equation 8 will have two unknowns and can not be solved alone. By combining two wires at an angle two one another, a set of two equations is obtained. To reduce the number of unknowns all angles and velocities are defined in the probe coordinate system, (x_p, y_p, z_p) rather than relative to the individual wire. The coordinate transformation will be discussed in section X. The reduction of unknowns results in a set of two equations and two unknowns. The equations are implicit but can easily be solved. An alternative to the effective angle method could be to tabulate f for different values of α. When the equations are to be solved one can first guess a value for α, use the corresponding

value of f and solve the equations. If the guessed angle and the calculated angle is equal, the final solution is found, if not another iteration is needed.

In the case of three dimensional flow the binormal cooling must also be considered. Equation 8 describes the effect of the normal and tangential cooling, and can be expanded by adding the binormal cooling on the right hand side of the equation. S is now the velocity component in the normal-tangential plane.

$$U_i{}^2 \cos^2(\alpha_{ei}) = S_i{}^2 \cos^2(\alpha_{ei} + \alpha) + U_{bi}{}^2 \tag{9}$$

The index i is used to refer to the different wires of the probe. $U(E_i)$ is obtained from the velocity calibration curve as a function of the wire voltage, E_i.

For a three wire probe we get a system of equations

$$U(E_1)^2 \cos^2(\alpha_{e1}) = S_1{}^2 \cos^2(\alpha_{e1} + \alpha) + U_{b1}{}^2 \tag{10}$$
$$U(E_1)^2 \cos^2(\alpha_{e2}) = S_2{}^2 \cos^2(\alpha_{e2} + \alpha) + U_{b2}{}^2 \tag{11}$$
$$U(E_1)^2 \cos^2(\alpha_{e3}) = S_3{}^2 \cos^2(\alpha_{e3} + \alpha) + U_{b3}{}^2 \tag{12}$$

To be able to solve this system the (x_p, y_p, z_p) coordinate system is used, the transformation from wire coordinate system to probe coordinate system is described in the next section.

2.1.3 Coordinate transformation

To reduce the number of unknowns in equation 10 it is necessary to express S_i and U_{bi} as functions of U,V and W which are defined in the probe fixed coordinate system, (x_p, y_p, z_p). Figure 3 defines the coordinate system and the angles needed to relate the probe wires to the coordinate system.

ϕ_i is the angle between the projection of wire i in the $(y_p - z_p)$ plane and the y_p axis. Figure 4 shows the projection of the wires in the $(y_p - z_p)$ plane and the corresponding ϕ angles.

If the wires are placed in a perfect triangle, the values of the angles will be $90°, 330°$ and $210°$ respectively. Two velocity components are defined in the $(y_p - z_p)$ plane, U_{bi} is the binormal cooling of wire i and U_{TPi} is the projection of the tangential cooling velocity of wire i, tp refers to tangential projection. U_{TP} and U_b can be calculated for the individual wires. They are functions of V,W and ϕ_i.

$$U_{TPi} = V \cos\phi_i + W \sin\phi_i \tag{13}$$
$$U_{bi} = V \sin\phi_i - W \cos\phi_i \tag{14}$$

The velocity component in the normal-tangential plane of wire i,S_i, is a function of U and the projection of the tangential cooling velocity.

$$S_i{}^2 = U^2 + U_{TPi}{}^2 \tag{15}$$

Substituting for U_{TP} in equation 15 yields S as a function of U,V and W.

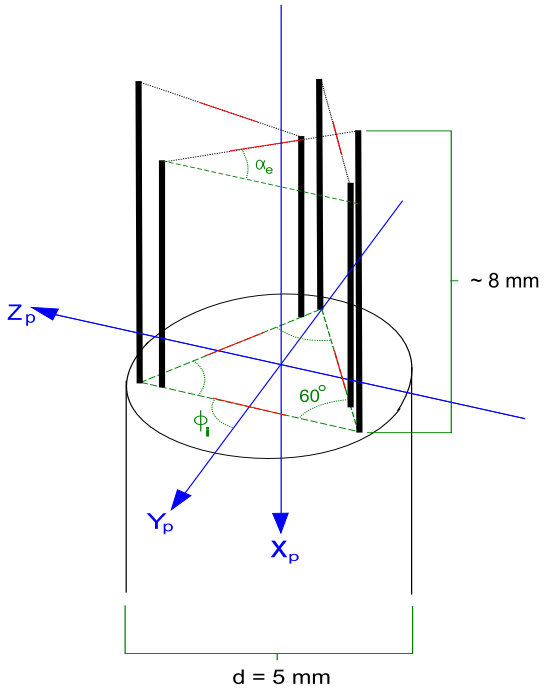

Figure 3: Definition of the angles relating the wires to the coordinate system

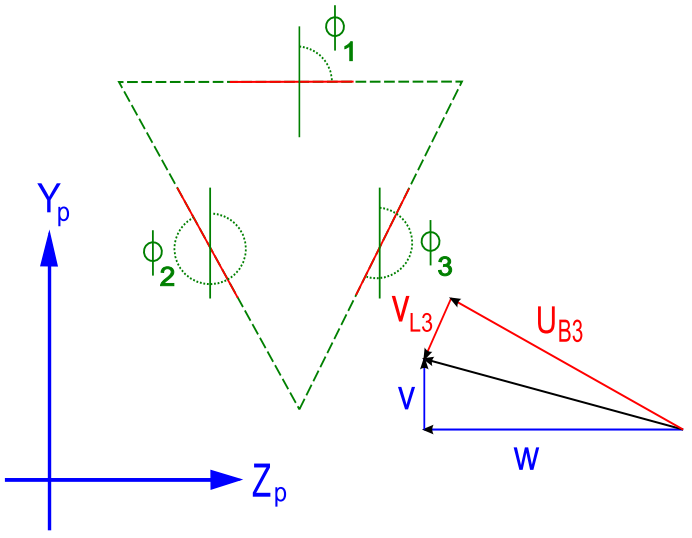

Figure 4: Velocities and angles in the $(y_p - z_p)$ projection

$$S_i^2 = U^2 + (V\cos\phi_i + W\sin\phi_i)^2 \tag{16}$$

The flow angle α in the normal tangential plane must also be defined. From figure X an expression for α is easily found.

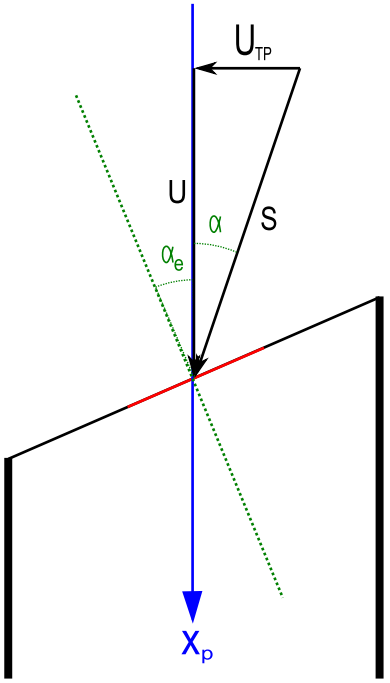

Figure 5: Definition of α

$$\alpha = \arctan\left(\frac{U_{TP}}{U}\right) = \arctan\left(\frac{V\cos\phi_i + W\sin\phi_i}{U}\right) \tag{17}$$

Equations 13, 15 and 17 may be substituted into equation 10 to yield the final equation for three dimensional flow over wire i.

$$\begin{aligned} {U_i}^2\cos^2(\alpha_{ei}) = {} & (U^2 + (W\cos(\phi_i) - V\sin(\phi_i))^2) \\ & +\cos^2\left(\alpha_{ei} + \arctan\left[\frac{W\cos\phi_i - V\sin(\phi_i)}{U}\right]\right) \\ & +(W\sin(\phi_i) + V\cos(\phi_i))^2 \end{aligned} \tag{18}$$

For the three wire probe a set of three equations with three unknowns is obtained.

2.1.4 Obtaining the angular response

For the individual wires the effective angle α_e must be found. This obtained by placing the probe in a uniform flow with a velocity S, and measuring the response for multiple yaw angles, α, while the pitch angle β is held constant at zero. Equation 8 describes the relation between the flow velocity and the velocity measured by the wire, U(E). The ratio between S and U(E) can then be found from equation 8.

$$\frac{U(E)}{S} = \frac{\cos(\alpha_e + \alpha)}{U(E)\cos(\alpha_e)} \tag{19}$$

The results from measurements at different angles α can then be curvfitted to equation 19 by adjusting α_e to obtain the best fit to the datapoints. A typical set of calibration angles is $\alpha = -20 : 5 : 20$. In section 2.1.2 α_e was presented as the geometric angle between the wire normal in the normal-tangential plane and the x_p axis. This is not entirely true, α_e will also be a function of the properities of the individual wire and most importantly of the flow angle. The effective angle approach assumes that the effective angle is constant, this is however not true for large flow angles. A litterature review by Lekakis [5] found several estimates of the limits for x-wire probes ranging from $\pm 12° - \pm 20°$. Russ and Simon found that the range of valid angles were larger for three-wire probes, in the range of $\pm 30°$(reported in the litterature review of Aanesland [1]).

2.2 Probe volume and frequency response

The spatial resolution is an important property of a measurement technique. All measurement techniques have a lower limit for spatial resolution, the variation is large. The spatial resolution of a pitot equals the diameter of the probe at least, for a laser doppler the size of the crossection of the laser beams is the limit, in particle image velocimetry it will depend on the window size and overlapping among other factors.

For a single subminiature hot wire Ligrani and Bradshaw [6] found the ideal ratio between wire length and diameter to be approximately $L/D > 260$ for $L < 1mm$ for measurents in a turbulent boundary layer. For longer wires 'eddy averaging' was reported. The wires used in this project is not close to the dimensions of the wires used by Ligrani and Bradshaw, and can therefore not be expected to resolve the smallest scales in the flow accurately. The physical size of the three wire probe will however be a greater limiting factor than the dimesions of the individual wires.

A velocity gradient across the measurement volume of the probe will mean that the wires in the probe experience different velocities. In a flow with a large velocity gradient, i.e. close to a wall, this can result in large differences across the probe volume and distort the result. The size of the probe volume will therefore limit how large gradients which can be measured.

The response of the individual wires is also important to obtain a good result. If the frequency response of the hot wire anemomters are different, some turbulent components can be overestimated. If for example the goal of an experiment is to validate whether a flow is isotropic or not, a difference in frequency response can

be a source of error. Most likely the three wires will not have identical frequency responses. To reduce the effect of this, the signals should all be filtered at the same cut off frequency.

2.3 Turbulent pipe flow

A confined flow such as a pipe flow will develop until a steady state solution is reached. Assuming that the flow entering the pipe is uniform, the boundary layer will immediately start to grow at the wall. The final steady state solution is reached when the inviscid core is gone, the flow is then said to be fully developed. The form of the velocity profile will depend on whether the flow is turbulent or laminar, the wall roughness and the pressure gradient.

Fully developed turbulent pipe flow will exhibit certain characteristics. In this section a brief review of some of these characteristics is given.

2.3.1 The pressure gradient

A uniform flow entering a pipe will be retarded by the shear stress from the walls. The pressure gradient will be greatest in the beginning, and gradually decrease until the flow is fully developed. At steady state the driving force of the pressure gradient will balance the shear stress on the wall.

$$\frac{\partial P}{\partial x} = \frac{\tau_w 4}{D} \tag{20}$$

The wall shear stress can be related to the wall-friction velocity, u_*, which is an important parameter in pipe flow.

$$\tau_w = \rho {u_*}^2 \tag{21}$$

By combining equation 20 and 21 the wall-friction velocity can be found from the pressure gradient.

$${u_*}^2 = \frac{\partial P}{\partial X}\frac{D}{4\rho} \tag{22}$$

2.3.2 Mean velocity profile

A turbulent pipe flow will consist of three regions.

- An inner layer close to the wall where viscous shear is dominating
- An outer layer where turbulent shear is dominating
- An overlap layer merging the two layers together, where both types of shear is important.

The different regions of the pipe flow can be analyzed in several ways. A common approach is to identify the important parameters in the different regions and apply dimensional analysis. In the inner region the velocity is assumed to depend on the wall shear, fluid properties and the distance from the wall. Free stream conditions are assumed not to be important. The wall shear will however depend on freestream properties such as the pressure gradient.

$$\bar{u} = f(\tau_w, \rho, \mu, y) \tag{23}$$

Dimensional analysis yields two dimensionless parameters.

$$\frac{\bar{u}}{u^*} = f\left(\frac{yu^*}{\nu}\right) \tag{24}$$

The two dimensionless groups are denoted u^+ and y^+ respectively, giving $u^+ = f(y^+)$. In the inner viscous shear dominated region turbulent shear can be neglected. Analysis of the momentum equation will then yield that $u^+ = (y^+)$, see e.g. White [12]. In the outer region of the pipe flow the velocity no longer depends on viscous shear, but on the freestream pressure gradient and the radius of the pipe, R.

$$U_{cl} - \bar{u} = f(\tau_w, \rho, R, \frac{\partial P}{\partial x}), y \tag{25}$$

Dimensional analysis yields three dimensionless groups.

$$\frac{U_{cl} - \bar{u}}{u^*} = g\left(\frac{y}{R}, \frac{R}{\tau_w}\frac{\partial P}{\partial x}\right) \tag{26}$$

Somewhere between the inner and outer layer, the two layers must merge, giving the same velocity. At a given axial position in the pipe, the shape of g is assumed to be a function of $\xi = \frac{R}{\tau_w}\frac{\partial P}{\partial x}$. The overlap law for a given ξ can then be found by manipulating equation 24 and 26.

$$\frac{\bar{u}}{u^*} = f\left(\frac{yu^*}{\nu}\right) = \frac{U_{cl}}{u^*} - g\left(\frac{y}{R}\right) \tag{27}$$

The two regions can only be merged if the f and g are logarithmic functions. The resulting relation can be written both in terms of inner and outer variabels.

$$\frac{\bar{u}}{u^*} = \frac{1}{\kappa} ln \frac{yu^*}{\nu} + B \tag{28}$$

$$\frac{U_{cl} - \bar{u}}{u^*} = -\frac{1}{\kappa} ln \frac{y}{R} + A \tag{29}$$

Different values have been suggested for the constants κ and B, but they are considered to be nearly universial. A will depend on ξ.

2.3.3 Turbulent shear stresses

In a fully developed pipe flow the only mean velocity component is that in the streamwise direction, U. In section 2.3.2 it was showed how U varies as a function of y. The shear stresses in a flow are closely linked to the mean velocity gradients. The generalized Boussinesq eddy viscosity hypothesis suggests a relation.

$$\overline{u_i u_j} = \nu_T \frac{\partial U_i}{\partial x_j} - \frac{2}{3}\rho k \delta_{ij} \tag{30}$$

Based on equation 30, one can make som assumptions on the magnitude of the shear stresses in a pipe flow. The only mean velocity gradient is $\frac{\partial U}{\partial y}$, one would therefore expect $\overline{uv}$ to be the dominant shear stress in the flow.

The variation of $\overline{uv}$ as a function of y can be found from manipulation of the Reynolds averaged Navier-Stokes equations. Equations 31 and 32 show the simplified RANS equations for the pipe flow.

$$\frac{\partial p}{\partial x} = \frac{\partial}{\partial y}\left[\mu \frac{\partial U}{\partial y} - \rho \bar{uv}\right] \tag{31}$$

$$\frac{\partial p}{\partial y} = \frac{\partial}{\partial y}\left[-\rho \bar{v^2}\right] \tag{32}$$

By integrating equation 32 with respect to y, from 0 to y an expression for the pressure at a given y coordinate is found.

$$\frac{P}{\rho} + \bar{v^2} = \frac{P_0}{\rho} \tag{33}$$

If one takes the derivative of the pressure with respect to x one will find that $\frac{\partial P}{\partial x}$ is constant with respect y, seeing that $\overline{v^2}$ is not a function of x.

$$\frac{\partial P}{\partial x} = \frac{\partial P_0}{\partial x} \tag{34}$$

The equation in the x-direction can be integrated in the same manner, with respect to y from 0 to y. By using the fact that $\frac{dP}{dx}$ is constant the following expression is found.

$$\frac{\partial P}{\partial x} y = \mu \left(\frac{\partial U}{\partial y}_y - \frac{\partial U}{\partial y}_0 \right) - \rho \overline{uv} \tag{35}$$

Substituting equation 21 for $\frac{dU}{dy}_0$ yields the following equation.

$$0 = \frac{y}{\rho}\frac{\partial P}{\partial x} + \frac{\mu}{\rho}\frac{\partial U}{\partial y} - \overline{uv} - {u_*}^2 \tag{36}$$

At the center of the pipe at $y = h$, $\frac{\mu}{\rho}\frac{dU}{dy} - \bar{uv} = 0$ due to symmetry. By using the known situation at the center line an expression for the variation of the total stress can be found as a function of y.

$$-\overline{uv} + \frac{\mu}{\rho}\frac{\partial U}{\partial y} = {u_*}^2\left(1 - \frac{y}{h}\right) \tag{37}$$

Equation 37 provides valuable information about how $\overline{uv}$ vary as a function of y. In the inviscid region viscous shear stress is neglible and the turbulent shear stress is expected to vary linearly with respect to y. And at the center line all shear stresses are expected to be zero.

2.3.4 Turbulent normal stresses

Boussinesq estimates the normal stresses to be one third of the turbulent kinetic energy k. In turbulent pipe flow that is not the case. Equation 30 assumes isotropic and homogeneous turbulence, but in a shear flow the production of the normal stresses will vary. In the case of a turbulent flow the turbulent kinetic energy equation in the axial direction will be the only one with a production term.

$$Production = -\overline{uv}\frac{\partial U}{\partial y} \tag{38}$$

The production depends on the mean flow gradient, as mean velocity in the y and z direction is zero for a fully developed pipe flow the production of the turbulent normal stresses is zero. This does not mean that the other normal stresses will be zero. Energy is transfered from $\bar{u}^2$ to $\bar{v}^2$ and $\bar{w}^2$ by nonlinear pressure-velocity interactions [8].

2.4 Cylinder wake

The cylinder wake is a complex and Reynolds number dependent flow. For very low Reynoldsnumbers, Re < 49, a laminar, symmetrical and steady recirculation region is present behind the cylinder. As the Reynoldsnumber increases laminar vortex shedding will begin. When the Reynoldsnumber reaches about 194 streamwise vortices begin to form [4]. Up to about $Re_D = 1000$ the Strouhal number increases [11]. The Strouhal number is defined as the ratio between fD and U, where f is the vortex shedding frequency behind the cylinder.

$$St = \frac{fD}{U} \tag{39}$$

For $Re_D > 1000$ the Strouhal number start to decrease untill it stabilizes for $10000 < Re_D < 100000$ at a value close to 0.21 [11]. The region from $Re_D = 1000$ to $Re_D < 200000$ is named the subrcritical range [13]. In the subcritical range the boundary layer on the cylinder remains laminar. If the Reynoldsnumber increases further the boundary layer starts to develop from laminar to turbulent, moving the point of transition upstream and the separation point downstream. This results in reduced drag and a narrowed wake.

Unlike a pipe flow, the wake is continually evolving. The mean velocity field will continue to develop until free stream conditions are reached. Momentum is continually transported towards the center of the wake where the velocity deficit is

largest. This can be seen from the continuity equation, which in its incompressible form yields the following.

$$\frac{\partial V}{\partial y} = -\frac{\partial U}{\partial x} \tag{40}$$

The continuity equation tells us how the gradient of V with respect to y is expected to vary. Far from the centerline $\frac{dU}{dx}$ will be negative, since the wake is expanding. In this region $\frac{dV}{dy}$ will be positive. Closer to the center of the wake we expect $\frac{dU}{dx}$ to be positive, $\frac{dV}{dy}$ must therefore be negative.

By performing an order of magnitude analysis, the x-direction Reynolds averaged Navier-Stokes equation can be simplified considerably. The two dominant terms are the U gradient with respect to x and crossectional gradient of the turbulent shear stress $\overline{uv}$.

$$U\frac{\partial U}{\partial x} = -\frac{\partial}{\partial y}(\overline{uv}) \tag{41}$$

Far downstream from the cylinder ($x/D > 80$) the flow can be assumed to be self-preserving [ref], which means that the shape of the profile is preserved along the x-axis. The shape of the profile can be found by starting with equation 41 and making some additional assumptions.

3 Experimental setup and procedure

3.1 The hot-wire probe

The probe consist of three wires on six supporting prongs, as shown in figure 3. The chosen geometry is defined by two properties:

- The projection of the wires in the $y_p - z_p$ plane is a triangle with 60 degree angles
- The wires are inclined an angle $\alpha_e = 35.26°$ relative to the $y_p - z_p$ plane

These properties give a geometry where the wires are orientated perpendicular to one another. The geometry is the same as recommended by Aanesland [1]. It was chosen to reduce the probe volume and give a good cooling response in all directions. The probes are manufactured to fit the above description, but the angles will never be exactly correct. The effective angles must be found trough the procedure described in section 2.1.4. By taking a picture of the probe trough a microscope, the orientation of the wires in the $y_p - z_p$ plane can be found, such a photo can be seen in figure 6. The angle ϕ_1 is used to relate the rotation of the probe in the $y_p - z_p$ plane to coordinate system.

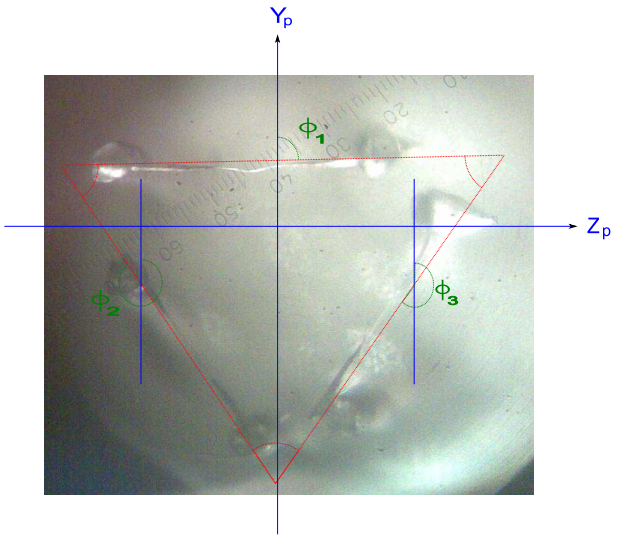

Figure 6: Picture of the $y_p - z_p$ plane taken trough a microscope

The length of the supporting prongs is chosen such that the flow over the wires are not influenced by the rest of the probes. It is also important that the prongs are not too long, as this can cause vibrations which in turn can be interpreted as a turbulent velocity component.

A platinum(90 %) , rhodium(10 %) alloy is used in the wire. This alloy gives a good oxidation resistance, relatively high tensile strength but has a relativly low

temperature coefficient of resistance making it less sensitive to velocity change [2]. The diameter also influences the sensitivity of the probe. In this project a wire with d = $5\mu m$ is used. This is a relativley thick wire, which reduces sensitivity but increases mechanical strength. The length of the wire between the probes is approximatly 4 mm, of this approximatly 1.75 mm of the coating on the wire has been etched away in the centre. This gives $l/d \approx 350$. To reduce the interference on the flow from the supporting prongs the distance between the supporting prongs should not be to small, the shape of the prong tips will also affect the flow [2].

The crossection of the measurement volume is ≈ 5 mm, and the spatial resolution of the probe is there for assumed to be 5 mm.

3.2 Measurement chains

Figure 7 describes the measurement chain in the experiment.

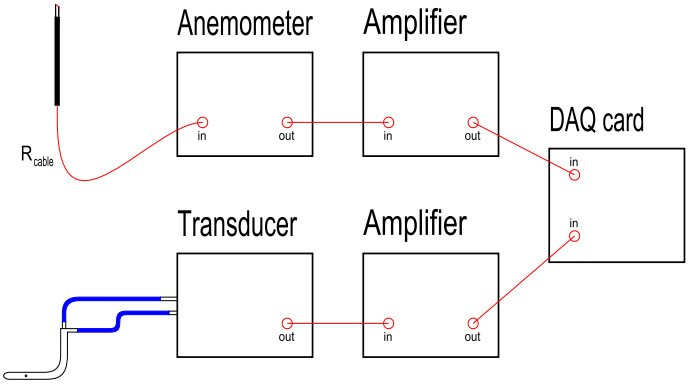

Figure 7: Measurement chain

The hot wire anemometers are optimized for $1\mu m$ not for $5\mu m$ which is used in this experiment. For the initial measurement setup a high frequency disturbance appeared on the signal at high velocities ($> 12m/s$). This is a result of the inability of the control circuit to regulate the wire voltage. It could to a certain degree be helped by changing the bias setting on the anemometer. This increased the damping in the control loop at the cost of a lower frequency response. For the pipe measurements this was sufficient, in the cylinder wake however the large fluctuations required that higher velocities could be measured. The solution was to extend the cable, increasing R_{cable}, and thereby increasing the damping in the loop.

3.3 Signal sampling rate

The sampling rate must be set according to the timescale of the smallest eddies of interest. When the range of timescales expected is unknown, the sampling rate must be set according to the smallest timescale on can expect. Kolmogorovs micro

scales are the smallest scales present in a flow. They can be estimated, this has not been done in this project.

The limiting factor for the sampling rate is in this case is the frequency response of the anemometers. The frequency response was found to vary between the wires from approximatly 6.3 kHz to 8.0 kHz. A low pass filter cut off frequency of 6.5 kHz was chosen. The sampling rate should be set according to the sampling rate theorem or Nyquist criteria, which states that the sampling rate should be greater than twice the maximum frequency expected to avoid aliases [10].

A suitable sampling time should be chosen such that repeated measurements give the same result, averaging over relevant timescales in the flow.

In the cylinder wake measurements a sampling rate of 13 kHz was used along with a sampling time of 20 seconds. For the pipe measurements the sampling frequency was set to 7 kHz and the sampling time to 10 seconds. This was not intended to be the final measurements, but simply preliminary measurements, the reduced number of datapoints gave significantly reduced datasize and was therefore chosen at the time.

3.4 Data reduction program

The sampled signal from the velocity calibration, the effective angle calibration and traverses, were stored in text files and imported into a Fortran script. The script corrects the data for temperature change, fits polynomials to the velocity calibration data, calculates the effective angles, and uses the calibration data to calculate timeseries of velocity vectors from the voltage timeseries.

The solution of the equations (Eqs. 18) was be found by using a zero point finder. Initially a fortran function called DNSQE from the SLATEC library was used, this function had previously been used by Aanesland [1] with success. The algorithm worked fine for averaged voltages, but convergens problems arised when the turbulent timeseries were analyzed. As an alternative Matlabs fzero function was used. The Matlab function is considerably slower than the Fortran routine but it does the job. Simple constraints were placed on the solution to insure that a physically correct solution was found. The Fortran script used for data analysis is described furher in appendix 6.

3.5 Pipe flow rig

The pipe rig consists of a hydraulically smooth PVC pipe, with a diameter of 186 mm and a length of 83 diameters. Ten pressure taps are mounted on the pipe, making it easy to measure the pressure gradient. The pipe is fitted such that a traverse can be mounted on top, making it possible to traverse the flow through the center of the pipe. Velocities in the pipe rig could be varied from 5 to 12.5 m/s.

The coordinate system used in the pipe has its reference($y = 0$) on the centre line of the pipe, y is positive above the centerline, and negative below the centreline. The velocities in the pipe are denoted U_x,U_r and U_{theta} and are the axial, radial and circumferential velocities respectively.

3.6 Wind tunnel

An open loop wind tunnel is used for the cylinder wake measurements. The test section is 45 cm x 45 cm and 110 cm long. A cylinder with a diameter of 47.5 mm is fitted in the center of the test section, leaving 50 cm of distance downstream for the flow to develop. Measurements are taken at $x/D = 10$. Velocities in the windtunnel could be varied from 4 to 30 m/s.

In the wind tunnel the centre of the wake is the reference($y = 0$) in the coordinate system, y is positive above the centerline, and negative below the centerline. U,V and W are the axial, vertical, and transverse velocity components respectively.

4 Results and disscusion

4.1 Calibration and testing

4.1.1 Velocity calibration

In the pipe rig the velocity calibration was performed for velocities between 5 and 12.5 m/s. A third order polynomial fit to the calibration data including the zero velocity point gave a residual of the order of $10^{-}1$, while a second order fit to the data without the zero velocity point gave a residual of the order of $10^{-}3$. A second order polynomial was therefore found most suitable for velocity calibration in the pipe rig. The residual is defined as the sum of the relative deviations between the polynomial fit and the fitting data.

In the wind tunnel the velocity ranged from 4 to 30 m/s. Figure 8 shows the distribution of the measured velocity in a point in the cylinder wake.

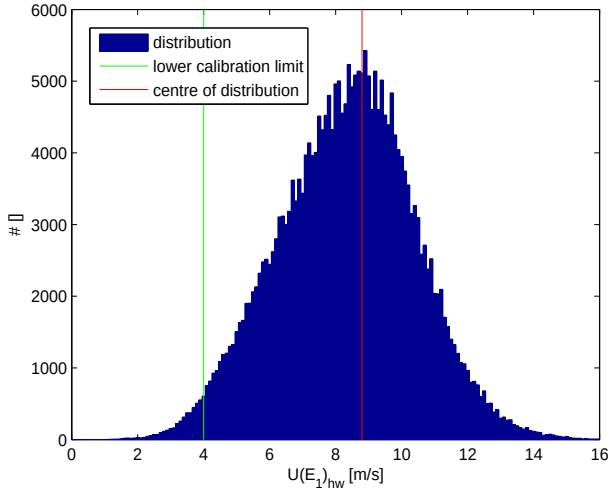

Figure 8: Distribution of streamwise velocity,U, in a measurement point in the wake behind a cylinder

The velocity scatter falls under the lowest freestream velocity obtainable in the windtunnel. This is not ideal as the polynomial fit in that region most likely will cause an error in the estimated velocity but it could not be avoided. A third order polynomial fit to the calibration data including the zero velocity point was chosen and gave a residual of $10^{-}1$. The match between the polynomial fit and the calibraton data for wire 1 is shown in figure 9.

4.1.2 Effective angle calibration

Figure 10 shows the cosine fitting of the effective angle calibration data.

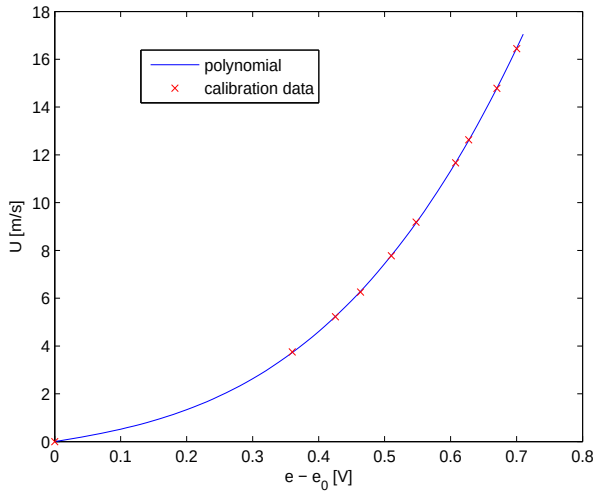

Figure 9:

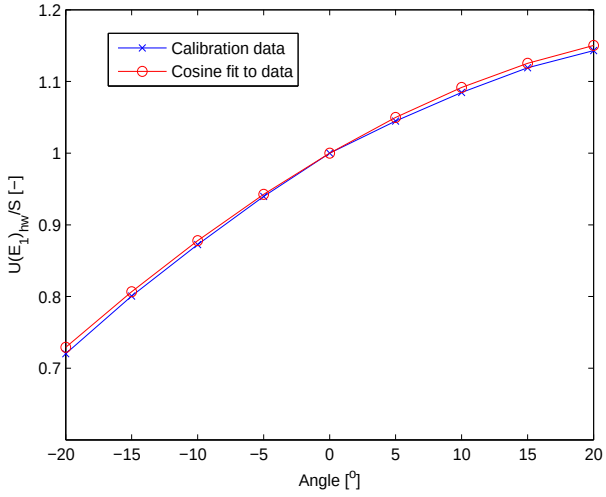

Figure 10:

Wire	α_e
1	31.69
2	35.88
3	35.64

Table 1: Effective angles found from calibration

True angle	U_{pitot}	U	V	W	Calc.angle	$\|V\|$	Rel.error
-20.00	9.9692	9.3490	0.4565	-3.5968	-21.05	10.0275	0.0058
-15.00	9.8884	9.6096	0.4545	-2.7205	-15.81	9.9976	0.0110
-10.00	9.9434	9.7241	0.4218	-1.7365	-10.13	9.8869	0.0057
-5.00	9.9169	9.8504	0.2921	-0.8429	-4.89	9.8907	0.0026
0.00	9.9007	9.8726	0.1849	0.1024	0.59	9.8749	0.0026
5.00	9.9608	9.8039	0.1368	0.9367	5.46	9.8495	0.0112
10.00	9.8936	9.6796	0.0971	1.7844	10.45	9.8431	0.0051
15.00	9.9672	9.5099	0.1003	2.6105	15.36	9.8622	0.0105
20.00	9.9852	9.2656	0.1193	3.3928	20.12	9.8680	0.0117

Table 2: Test of solution on dataset for wire 1

The residuals of the curvefit for the wires was of order 10^-2. The effective angles given by the calibration is given in table 1.

The angles are in the vicinity of the ideal value of 35.26° and vary within an aceptable range. To test the effective angles and the ϕ angles the data set from the angle calibration of wire 1 can be solved. Table 2 shows the true flow angle, the U velocity measured by the pitot, the calculated velocity components, the calculated α, the length of the calculated velocity vector and the relative error between the velocity measured by the pitot and the length of the calculated velocity vector.

Table 2 shows that the calculated α falls within $\pm 1°$ of the true flow angle. The relative error between U_{pitot} and $|V|$ is 1.2% at most. The Y_p component velocity, V, should be zero but shows a variation with respect to α. The maximum value of V corresponds to a flow angle of 2.9° or a 4.7% relative error, which is a relativly large error. The variation in V corresponds to an angle of 2.2°. Aanesland [1] performed the same measurements, and reports a $3-4\%$ relative error in V and W for similar conditions.

The large deviation seems to be a combination of misalignment of the probe relative to the flow and a dependency of the solution on the true flow angle. A probe pitch angle different from zero would give the misalignment, producing a permanent offset. The variation with α is most likely caused by a wrong value chosen for ϕ_1, since ϕ_1 is determined by visual observation and is not likely to be exact. The variation in V could be used to find the correct value of ϕ_1, the calculations could then be rerunned, and the remaining constant error in V should be caused by the pitch. Such a procedure has not been attempted in this project. Several authors, i.e. Cantwell and Coles [3] uses yawing to perform similar corrections, Cantwell and Coles used it for a x-wire probe.

4.2 Turbulent pipe flow

Two profiles of the turbulent pipe flow has been taken at a Reynoldsnumber of a approximately 10^5. The main difference between the two profiles is that they are taken at two different values of ϕ_1. This is done to investigate the effect of rotating the probe.

4.2.1 Pressure gradient

The static pressure in the pipe is measured using the pressure taps distributed along the pipe. Instead of measuring the absolute static pressure, the pressure difference is measured between the different points and a chosen reference point at $X/D = 70.5$. Figure 11 shows the drop in static pressure along the pipe. The line drawn in the plot is a straight line from the first measurement to the last.

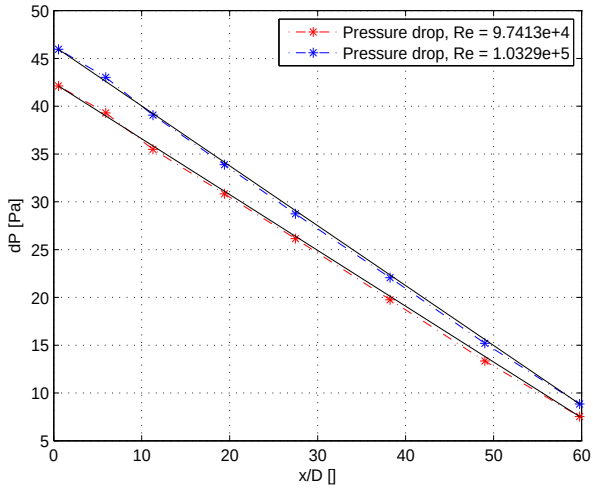

Figure 11:

As expected the highest Reynoldsnumber gives the biggest pressure drop. Both measurement series show a nearly linear drop in pressure, as one would expect for a fully developed flow. The pressure gradient is approximated by considering the pressure drop from $X/D = 11.3$ to $X/D = 70.5$. Based on the pressure gradient the friction velocity may be found from equation 22. The friction velocity can also be estimated from the friction factor,f.

$$u^* = U_{avg} \left(\frac{f}{8}\right) \frac{1}{2} \tag{42}$$

When the Reynoldsnumber and the roughness height of the pipe wall is known the friction factor can be found from the Moody diagram or from an equation. The PVC pipe is hydraulically smooth, and the friction factor can therefor be found

ϕ_1	Re_D	$\frac{dP}{dx}[Pa/m]$	$u^*{}_{\frac{dP}{dx}}[m/s]$	$f_{Re_D}[-]$	$u^*{}_{f_{Re_D}}[m/s]$
90	9.74×10^4	3.2236	0.3534	0.0181	0.3736
180	1.03×10^5	3.5487	0.3708	0.0179	0.3937

Table 3:

from Prandtls equation for smooth pipes [11]. Table 3 gives the results for the different values of ϕ_1

The two means of calculating the friction velocity gives similar results, the values given by the friction factor are about 6% higher than that given by the pressure gradient. In the following the friction velocity obtained from the pressure gradient is assumed to be correct.

4.2.2 Mean velocities

Figure 12 shows the velocity profile for the axial velocity U_x, for both $\phi_1 = 90$ and $\phi_1 = 180$.

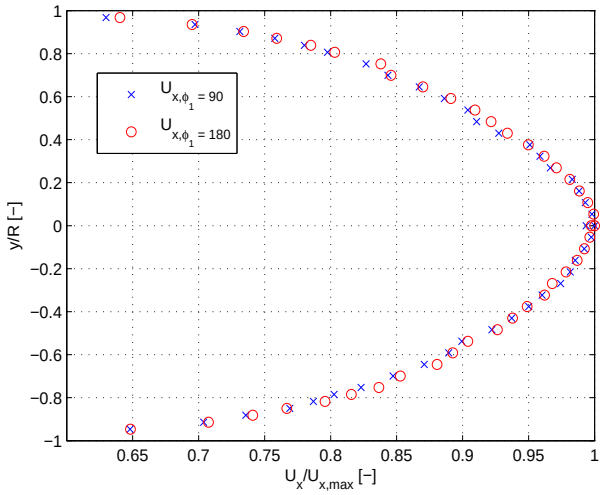

Figure 12: Normalized mean profile,U. $U_{x,max,\phi_1=90} = 8.75m/s$, $U_{x,max,\phi_1=90} = 9.25m/s$

The velocity on the centerline was measured a second time after the profile was taken, the result was within 1% of the first measurement for both profiles. Both profiles have the same shape.

In figure 13 the data for $\phi_1 = 90$ and $\phi_1 = 180$ is plotted against the logarithmic law. Torbergsen [9] did measurements in the same pipe rig for $Re = 75000$ and obtained a good fit with the logarithmic law using $\kappa = 0.41 and B = 5.5$. White [12] claims that $\kappa = 0.41 and B = 5.0$ give a better fit to experimental data. Both

versions of the logarithmic law is plotted in figure 13. The slope of the measurement data matches the choice of $\kappa = 0.41$. B = 5.0 as suggested by White gives the best fit to the measurement data in the log-law region.

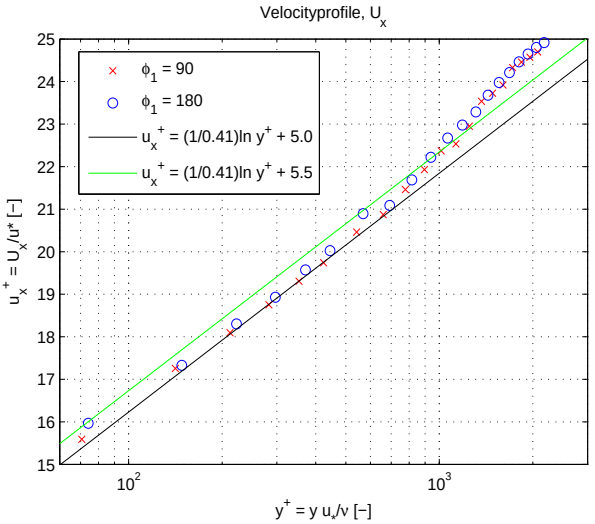

Figure 13: Logarithmic region

In a fully developed turbulent pipe flow one would expect the transverse velocity components U_r and U_θ to be zero. Figures 14 and 15 show that neither of the velocity components are exactly zero across the pipe. The radial pipe velocity U_r, is fairly constant over the cross section of the pipe, but show some variation, especially close to the pipe walls. The range of variation in velocity is about $\pm 0.125 m/s$ or approximately an angle of $\pm 0.8°$ relative to the average axial velocity. Both the profiles for $\phi_1 = 90$ and $\phi_1 = 180°$ show the same kind of variation with respect to y/R but they are offset relative to one another. The offset equals about 1.6° of probe pitch, which is within the error range one must expect when the probe is aligned with the flow visually.

The circumferential velocity U_θ show a peculiar variation over the crossection of the pipe, varying over a range of $\pm 0.45 m/s$ or $\pm 2.86°$ relative to the average velocity. If the deviation of the circumferential velocity is compared to the local axial velocity the range of angle variation exceeds $\pm 4°$, this is shown in figure 16.

The variation of U_θ with respect to y/R follows the same pattern for both series of measurements and closely resembles a typical inverse tangent function. If the variation were to be explained physically it would imply that the flow inside the pipe was rotating about the centerline. The velocity does however not decrease close to the wall, but increases rapidly, this implies an unphysically large shear stress on the wall.

Since the flow is assumed to be unphysical the radial variation must be caused by one or more errors in the setup, data reduction or caused by limitations of the

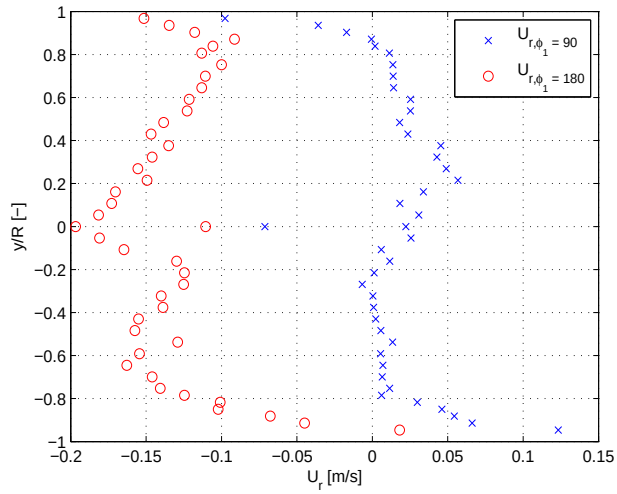

Figure 14: Radial mean velocity,U_r

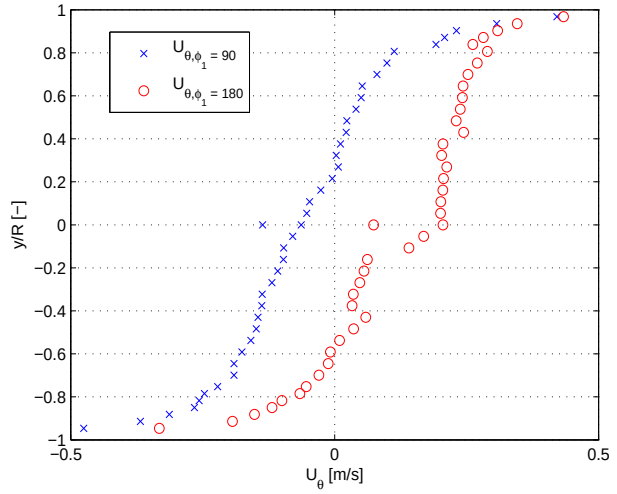

Figure 15: Circumferential mean velocity,U_θ

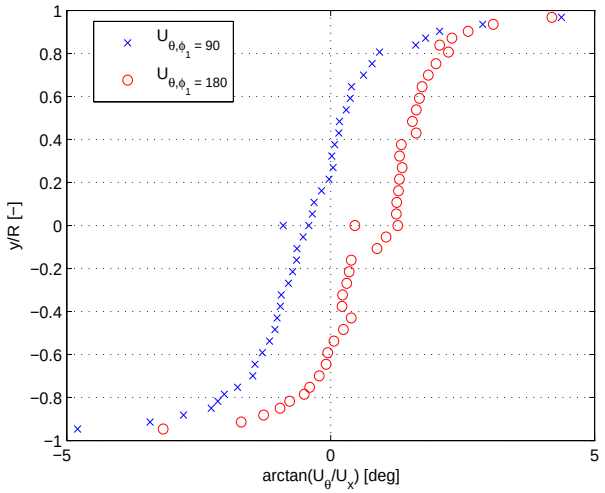

Figure 16: Circumferential mean velocity,U_θ, expressed as angular deviation relative to U_x

probe. The distinct shape of the profile can make one wonder if this variation could be linked to an error in the arctan expression in equation 18, but no such error has been found. An interesting observation can however be made by observing the difference in the two centerline measurements, both for U_r and U_θ the relative error between the two centerline points is large. While the repeated measurements gave solutions for the axial velocity U_x within one percent of the first solution, the radial and circumferential repeated solutions can vary up to 0.5° and 1° respectively. This is a large deviation compared to the range of the calculated values for U_r and U_θ. By re-examining the measurement data there was found to be a small drift in wire voltage, which could not be corrected for by considering the temperature change. Ideally the measurement series should have been repeated, but the error was discovered to late. Based on this observation parts of the large variation for U_r and U_θ might be caused by voltage drift. The shape of the variation of U_r and U_θ does however seem to be a function of y or a some other property related to y, not only a possible voltage drift. But what property could that be? U_x is a function of y, but is symmtric about the centreline. The gradient of U_x also varies as a function of y but is not symmtric. In section 2.2 the possible error of measuring in large velocity gradients was dicussed, this could possibly be the cause. This discussion is continued in the next section on shear stresses.

4.2.3 Turbulent shear stresses

As discussed in section 2.3.3, the $\overline{u_x u_r}$ shear stress is expected to be the dominant shear stress and behave linearly across a large portion of the pipe crossection according to equation 37. Figure 17 shows the theoretical relation and the experi-

mental results.

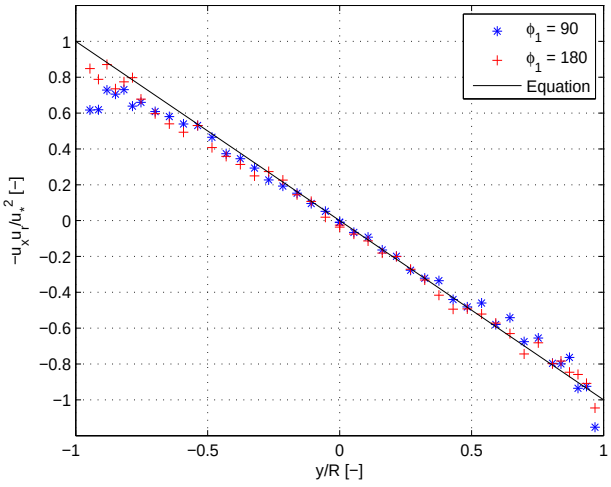

Figure 17: Turbulent shear stress $\overline{u_x u_r}/u^*$

The experimental results follow the linear relation well. The gradient is a bit smaller than 1 in the centre region where viscous shear is assumed to be neglectable but the deviation is small, a very similar result was found by Torbergesen [9]. At the centreline the measured shear stress is close to zero, as expected.

Close to the pipe wall the turbulent shear stresses are expected to decay and drop to zero in the viscous sublayer. The spatial resolution of the probe is not large enough to measure closer to the wall than about $y^+ = 70$ which is far outside the viscous sublayer. The measurement data show little tendency to drop of close to the wall. For $\phi_1 = 90$ there is a little drop for $y/R < -0.9$, while for $y/R > 0.9$ there is actually an increase in shear stress measured for both datasets. The increased shear stress could just be outliers, but it happens for both datasets.

The two other shear stresses, $\overline{u_x u_\theta}$ and $\overline{u_r u_\theta}$ should theoretically be zero as there is no mean velocity gradient resulting in production of neither of them. In figure 18 the normalized stresses are plotted. In the centre region the magnitude of $\overline{u_x u_\theta}$ and $\overline{u_r u_\theta}$ are relatively small compared to the maximum value of $\overline{u_x u_r}$, about 3%, but not zero. Moving closer to the wall both shear stresses increase slowly until $|y/R| \geq 0.8$, where the shear stresses increase more rapidly. The magnitude and variation of the shear stresses can not be explained physically, and must be related to the measurement process.

For $|y/R| \geq 0.8$ the velocity gradient experienced by the probe volume is large. The exact effect of an exessively large velocity gradient compared to the probe volume is unknown. But it will result in calculated velocities different from the true velocity, as the wall is approached. The result can be a gradient of both U_r and U_θ with respect to y as observed in section 4.2.2. Subsequently this is likely to

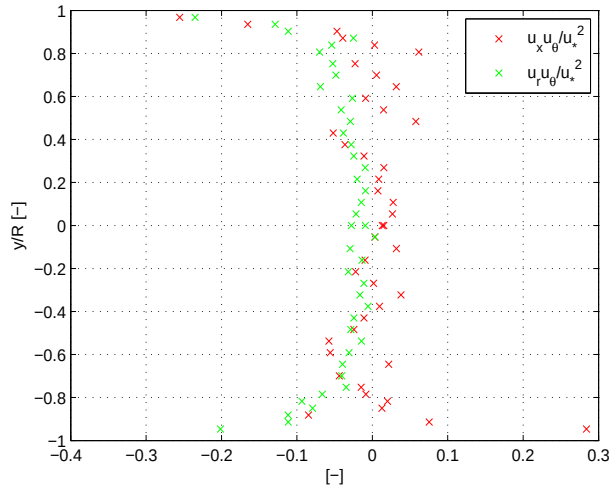

Figure 18: Shear stresses $\overline{u_x u_\theta}$ and $\overline{u_r u_\theta}$

result in unphysical shear stresses. In section 4.2.2 the deviation for both U_r and U_θ was found to increase rapidly for $|y/R| \geq 0.8$, this matches the result found for $\overline{u_x u_\theta}$ and $\overline{u_r u_\theta}$ and supports the theory that a large velocity gradient biases the result.

When comparing the results with that found by Aanesland [1], the data scatter for the profiles obtained in this project is larger and do not collapse as neatly into a line as the results of Aanesland. What causes this is uncertain, but a to short sampling time could potentially be the reason.

4.2.4 Turbulent normal stresses

Figure 19 displays the reduced normal stress for both measurement series, which reveals that $(u_x)^+$ is the largest normal stress, as one would expect.

Torbergsen [9] found ${u_x}^+$ on the centreline to be approximately 0.85 for $\Re = 0.75e5$. The results should be comparable as the Reynoldsnumbers is of the same order. According to the results of Torbergsen, ${u_x}^+$ is fairly constant on the centreline for increasing Reynoldsnumbers, but increases closer to the wall due to the increased velocity gradient. ${u_x}^+_{cl.} = 0.85$ matches the obtained results fairly well, there is however some scatter in the data as is already mentioned in the end of section 4.2.3. The dataseries for the two different probes also give slightly different results. Moving closer to the wall ${u_x}^+$ is underestimated compared to the results of Torbergsen, but matches the results of Aanesland [1] better. ${u_r}^+$ and ${u_\theta}^+$ show the same variation as reported by Torbergsen for $|y/R| \geq 0.6$ but the scatter is large for variation of ϕ_1.

Values for ${u_x}^+$,${u_r}^+$ and ${u_\theta}^+$ can not be estimated without giving a relativly large potential error. ${u_\theta}^+$ for $y/D = \pm 0.6$, can for instance be estimated as 1.1but

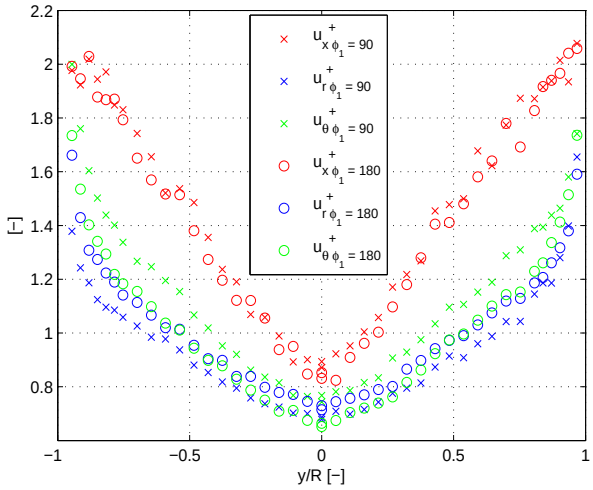

Figure 19: Reduced normal stress

the scatter is of the order 0.2, and could potentially be larger if measurements at more values of ϕ_1 were taken. The large varition can be caused by poor adjustment of ϕ_1, it is as mentioned earlier set visually.

In figure 20 the turbulence intensity relative to the local streamwise velocity is plotted.

The streamwise turbulence intensity on the centreline, ${u_x}^+ \approx 3.3 - 3.6$. Torbergsen reported a value of approximately 3.5%. On the centreline ${u_r}^+$ and ${u_\theta}^+$ should be equal due to symmetry, there is however some difference which is most likely caused by misalignement of the probe.

4.3 Cylinder wake

The cylinder wake can be analyzed both as a mean flow and as a time varying flow. Both approaches will be tested in this section. Ideally several measurement series for different values of ϕ_1 should have been taken to gain more information about the probe response. Only one measurement series was taken however. A velocity profile was taken in the test section before the cylinder was inserted, to map the reference free stream conditions.

Vortex shedding from a circular cylinder is a much studied flow, it did however prove difficult to find near wake results in the same range of Reynoldsnumbers(10^4), and downstream distance x/D. A survey using a four wire hot wire probe by Ong and Wallace at $\Re = 3900$ was the closest match found [7]. They used a four wire hot wire probe with a crossection of 1 mm x 1 mm. For the flow investigated in this project $\Re = 30717$, placing it in the subcritical range together with the results of Ong and Wallace. The results can therefore be assumed independent of

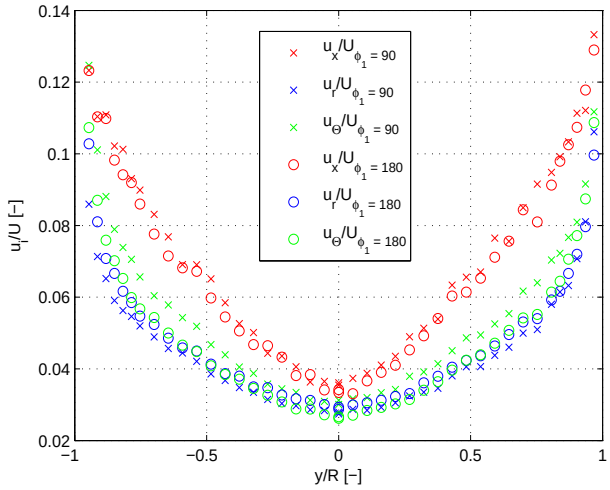

Figure 20: Turbulence intensity

Reynoldsnumber and comparable.

Emphasis is placed on assesment of the physical validity of the result, as well as comparison with the results of Ong and Wallace.

4.3.1 Mean velocity profiles

The profile of the streamwise component U is shown in figure 21, the velocities are plotted relative to the incoming velocity. From figure 21 one can see that the velocity in the wake exceeds the reference free stream velocity. This indicates there is a speedup effect caused by the cylinder. The average free stream velocity is $9.7m/s$ while the average velocity in the wake profile is $9.3m/s$. A lower average velocity in the wake means that the presence of the cylinder causes a blockage of the flow. The area of the crossection traversed does however not cover the entire crossection. Since the velocity in the wake profile is higher close to the wall, this means that the average velocity in the wake is higher than $9.3m/s$. By simply estimating the rest of the wake profile from the highest measured velocity in the wake, the average velocity in the wake is found to be $9.66m/s$. This means that blockage effects are neglectable, and that a reference velocity of $9.7m/s$ may be reasonable. Based on the reference velocity the Reynoldsnumber,Re_D, is calculated to be 30717.

As the cylinder wake is an evolving flow, V is not expected to be zero, due to the constraints of continuity. For a perfectly symmetrical wake V is expected to be zero in the center of the flow and negative over the symmetry line and positive below. The profile of V is plotted in figure 22, along with the free stream profile. Ideally the free stream conditions should be zero. Due to misalignment of the probe an offset from zero would not be unexpected, the velocity does however vary over

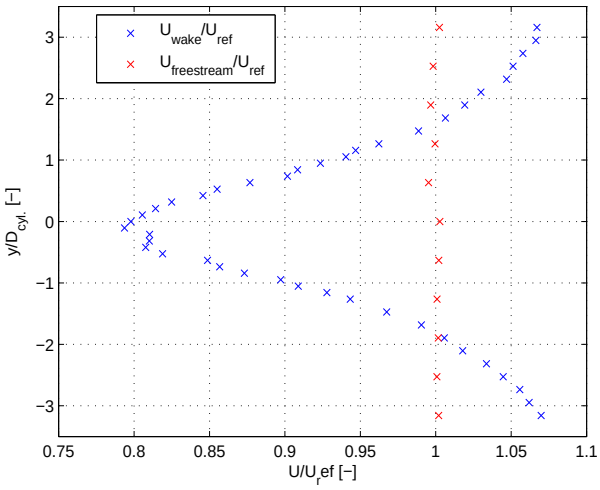

Figure 21: Normalized profile of U in cylinder wake for Re = 30717, x/D = 10

the crossection. Whether this is a true property of the flow or not is unclear, the range of variation in V equals 2.4 deg probe pitch relative to the reference velocity. If the velocity profile is corrected by subtracting the local freestream velocity, the profile will be as in figure 23. This correction assumes that the flow velocities can be superpositioned. The result looks more like what one would expect, but when compared to the results of others i.e. Ong and Wallace [7] the shape of the velocity profile is not a perfect match.

The velocity component in the z-direction is plotted in figure 24 along with the freestream measurements. The same velocity profile corrected for freestream conditions is plotted in figure 23.

The freestream velocity variation can not be explained by the finite size of the probe and it is not a constant offset as a yaw angle would give. The variation of W in freestream conditions is however rather small, it equals approximately 2°. In the wake of the cylinder the variation of W is sligtly larger.

It is not straightforward to understand how the timevarying velocity gradients in the wake of cylinder will affect the measurements. If the timeseries could be conditionally averaged on i.e. the pressure variation on the cylinder, the timeseries for different y coordinates could be linked, and the gradients found. Even if that could be done it is not straightforward to decide what effect it would have on the mean flow profiles. If the finite geometry of the cylinder and the wind tunnel affects the shedding process that could also cause three dimensional effects.

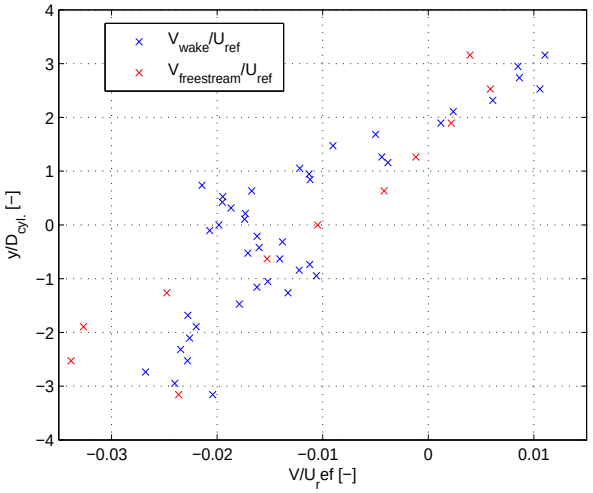

Figure 22: Normalized profile of V in cylinder wake for Re = 30717, x/D = 10

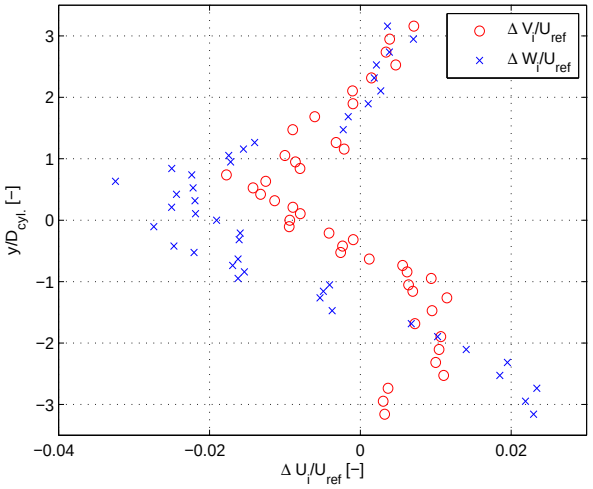

Figure 23: Normalized profile of $V - V_{freestream}$ and $W - W_{freestream}$ in cylinder wake for Re = 30717, x/D = 10

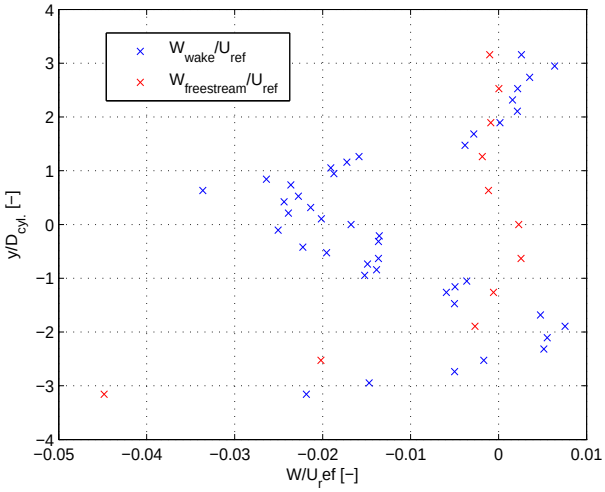

Figure 24: Normalized profile of W in cylinder wake for Re = 30717, x/D = 10

4.3.2 Turbulent shear stresses

The largest turbulent shear stress is again expected to be $\overline{uv}$ as it has the largest mean velocity gradient production term. In figure 25 the non-dimensionalized $\overline{uv}$ wake profile is plotted along with the freestream result.

The profile shows the same distinct shape found by i.e. Wissink and Rodi [13]. At the center where $\frac{\partial U}{\partial y}$ is zero, $\overline{uv}$ should be zero, the results show that $\overline{uv}$ validate this. The maximum/minimum values for $\overline{uv}$ is expected where the second gradient of U is zero. This occurs at $y/D \approx \pm 1$ and matches the mean velocity profile fairly well.

The sign of $\overline{uv}$ can be found from a simple consideration of the mean profile. If an air-particle at the upper half of the wake were to be given a negative turbulent velocity component, v', it would experience a positive streamwise turbulent velocity, u'. The product of these two would be negative, hence $\overline{uv}$ should be negative for the upper half of the velocity profile. If the particle is moved up instead the result is the same. The same line of reasoning will give a positive value of $\overline{uv}$ in the lower half of the wake.

Ong and Wallace found that the largest magnitude of $\overline{uv}/{U_{ref}}^2$ was about ± 0.004 at $x/D = 10$. From figure 25 one can see that the corresponding largest shear stress measured ranged from -0.005 to 0.008. The range of the variation is of the same order of magnitude, but it was expected that the variation would be symmetric about 0. The two other shear stresses are expected to be small for a 2D flow. Figure 26 shows the shear stresses, normalized by the reference velocity.

$\overline{uw}$ and $\overline{vw}$ are not negligibly small as expected, rather they are of the same order of magnitude as $\overline{uv}$. This can not be interpreted as a physically valid result,

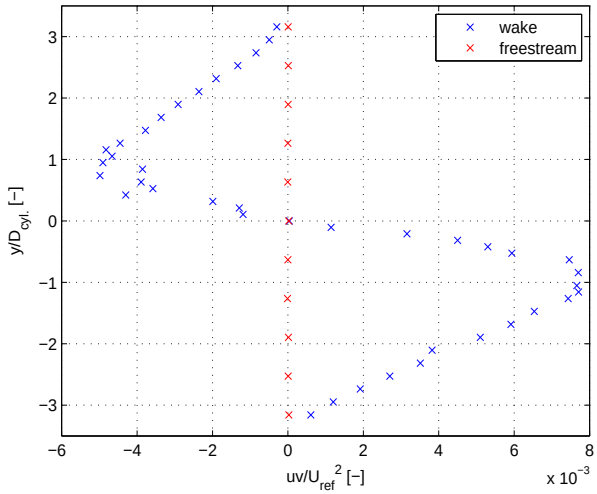

Figure 25: Profile of normalized turbulent shear stress $\overline{uv}$ in cylinder wake for Re = 30717, x/D = 10

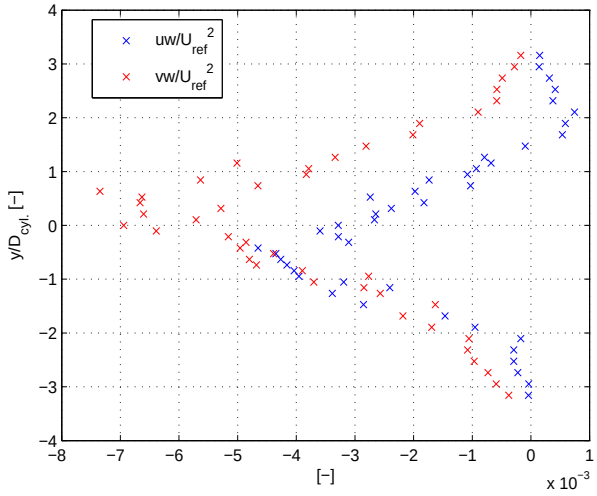

Figure 26: Profile of normalized turbulent shear stresses $\overline{uw}$ and $\overline{vw}$ in cylinder wake for Re = 30717, x/D = 10

but must caused by either the spatial resolution of the probe or some other factor in the measurement setup or processing.

4.3.3 Turbulent normal stresses

The largest normal stress measured in the turbulent wake is not the streamwise component but the crossflow normal stress $\overline{v^2}$. This in accordance with the results reported by i.e. Ong and Wallace [7]. The centreline streamwise turbulence intensity at $x/D = 10$ measured by Ong and Wallace is approximately 17% and flat in the centre region with a small reduction in turbulence intensity on the centreline. From figure 27 one can find that the centreline turbulence intensity is approximately 17.5%, which matches the result of Ong and Wallace but there is no reduction on the centreline. On the centreline Ong and Wallace found $\overline{v^2}/U_{ref}^2$ to be 0.083, from figure 27 a corresponding value of 0.06 is found, which gives a 28% deviation.

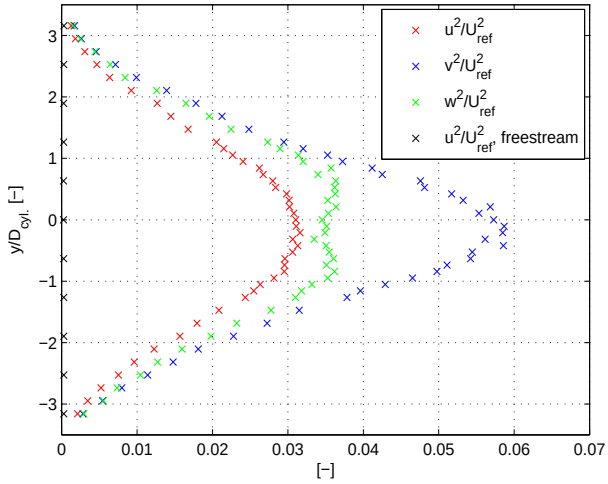

Figure 27: Profile of normalized turbulent normal stresses in cylinder wake for Re = 30717, x/D = 10

Ong and Wallace does not report the magnitude of $\overline{w^2}$ relative to the others. $\overline{w^2}$ exhibits a very characteristic platou in the centre region.

4.3.4 Analysis of the time varying wake

The vortex shedding behind the cylinder causes the velocity in the wake to vary in a orderly fashion as the vortices pass by. Figure 28 shows a small part of a solved timeseries on the centreline at $x/D = 10$.

All three velocity components exhibit variations in magnitude, but it is most clear for V, which show a periodic variation about a mean value close to 0. In a

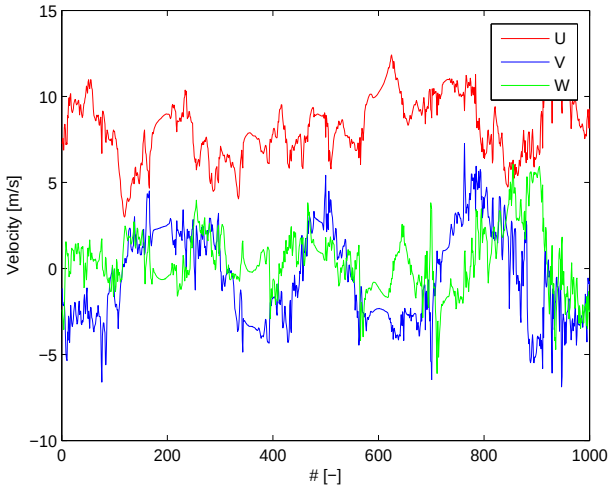

Figure 28: The solution of the first 1000 samples on the centreline at x/D = 10

perfectly two dimensional flow there should be no variation in W, which should be zero. From figure 28 one can however see that W varies over a range slightly smaller than that of V.

The frequency of the periodic variation of V can be found by analyzing the frequency content of the signal. This is done by taking a fast Fourier transform (FFT) of the dataset, the built in function in MATLAB is used for this purpose. Figure 29 shows the FFT of the solution of a timeseries measured at the centerline of V.

The FFT shows a clear peak at $f = 42.8Hz$. From equation 39 the shedding frequency can be estimated by assuming a Strouhal number of 0.21, and as previously mentioned the freestream velocity is assumed to be about $9.7m/s$.

$$f = \frac{0.21U}{d} = 42.9Hz \tag{43}$$

This is a very close match to the result of the FFT. It is however worth investigating the shedding frequency a bit closer. The analyzed dataseries is measured over a timeperiod of 20 seconds. If the vortex shedding process is perfectly stable, the peak frequency will be the shedding frequency. It is not likely that the frequency is completely stable but rather that it will vary slightly as a function of time. To investigate this, subsets of the measured data was investigated independently. Analyzing a subset of the measurement data will reduce the smoothing of the data and give a larger amplitude for the peak frequency. There is however an disadvantage of considering a small subset. When an FFT is found, the number of frequencies analyzed is taken as the largest power of two smaller than or equal to the sample size, this is done to increase the calculation speed. This means that the

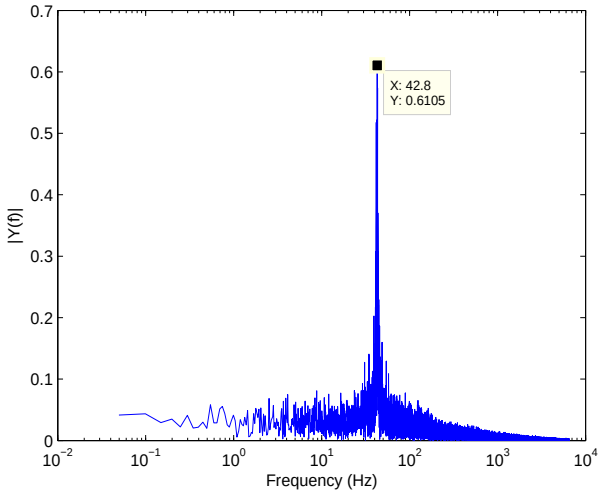

Figure 29: FFT of solution at centerline, x/D = 10, f_s 13000Hz, T_s = 20s

frequency resolution is reduced when the sample size is reduced. The timeseries is sampled at 13 kHz, the FFT can only find frequencies up to 6.5 kHz according to the Nyquist sampling criteria. To obtain a resolution of 1 Hz the FFT must be taken for 6500 frequencies. The smallest power of two larger than or equal to 6500 is $2^{13} = 8192$, which equals a 0.63 seconds sampling time, or approximately 26 shed vortices. Analysis of the first 0.63 seconds yield the FFT shown in figure 30. The shedding frequency was found to be almost the same, but the amplitude of the peak frequency is almost three times as large, indicating that frequency varies some over the span of one timeseries.

The shedding frequency can be used to conditionally average the signal by assuming that the shedding process is stable. This done by splitting the time period into N number of bins. A sampled timeseries is then analyzed, and the individual samples is placed in bins according to their temporal position relative to the other samples. In figure 31 the conditional average of U, V and W for the first second of a timeseries aquired on the centerline is plotted. The mean value of the different velocities is substracted. The data is conditionally averaged using half the calculated shedding frequency. I.e. the period averaged over equals the time it takes for two vortexes to be shed, one from each side of the cylinder.

The conditional averaging gives a clear variation of W with respect to the period over which the signal is averaged. The range of W is a bit smaller than that observed in figure 28. This indicates that variation is dampened by the conditional averaging process due to a varying shedding frequency. The variation in U and W is less systematic, but should be studied further. Several other interesting correlations could be investigated by conditional averaging, but there was not time for that.

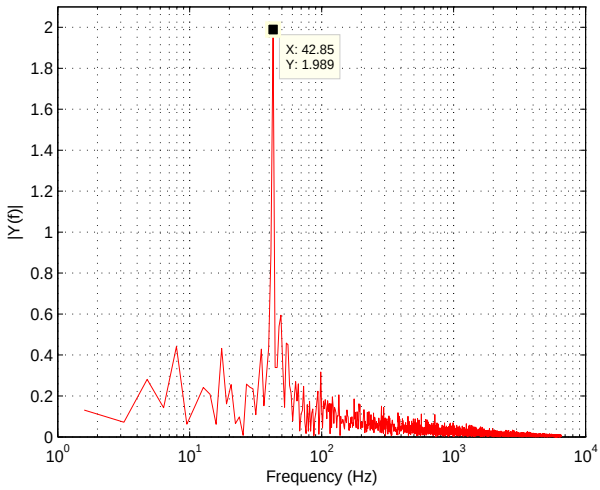

Figure 30: FFT of solution at centerline, x/D = 10, f_s 13000Hz, T_s = 0.63s

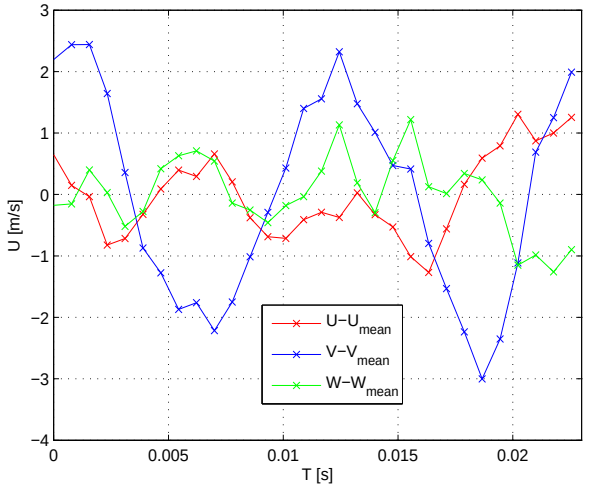

Figure 31: Conditional average of mean velocities, y/d = 0, 30 bins, 1 second

4.4 Performance of the probe

In this section an attempt to assess the properties of the hot wire probe based on the results presented is made. For the turbulent pipe flow the results were in reasonably good agreement with theory, major discrepancies were only found close to the pipe wall. Small errors most likely due to misalignment of the probe were observed at several occasions. From the effective angle calibration it was found that exact positioning of the probe visually could only be done with a limited accuracy. This affected the calculated properties, but must be expected. The normal stresses on the centerline of the pipe is such an example. Theoretically the crosstream normal stresses should be identical on the centerline, but due to misaligment of the probe the results deviated.

The discrepancies close to the wall are belived to be caused by the large velocity gradient. By making an estimate using a two-point numeric scheme the velocity gradient is found and plotted in figure 32.

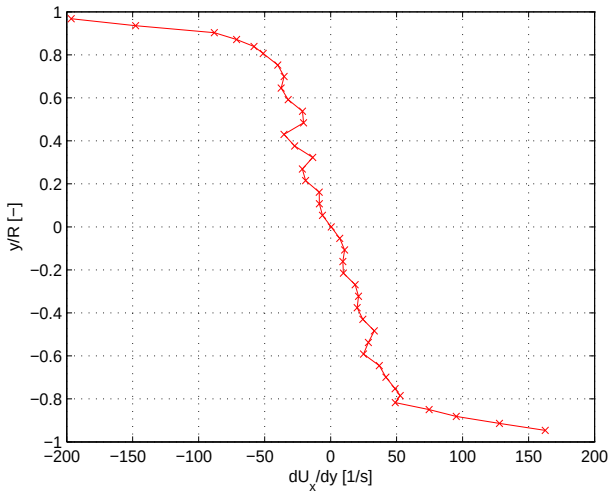

Figure 32: Gradient of U_x in the turbulent pipe flow

The shape of the velocity gradient profile look suspicously like the profile of U_r and U_θ. This strenghtens the hypothesis put forward in section X, that the variation of U_r and U_θ is linked to the velocity gradient. It is however worth noting that the two different values of ϕ_1 gives very similar results, it does however not seem obvious that the large velocity gradient will give the same error in both cases. Based on the profile for $\overline{uw}$ and $\overline{vw}$(figure 18) a rough estimate for the critical magnitude of the velocity gradient can be found. Assuming that the results are good until $|x/D| \geq 0.8$ the critical gradient can be estimated to be $\pm 50 s^{-1}$. Over the crossection of the hotwire probe this will equal a $0.25 m/s$ difference in velocity.

The next interesting question is of course what kind of gradients one can expect in the cylinder wake. As a start the gradient of the mean velocity field can be estimated. The result is plotted in figure 33. A maximum mean gradient of approximately $\pm 40 s^{-1}$ is found in the wake, which is just below what is estimated as a critical gradient. The maximum value of the gradient could be larger than $\pm 50 s^{-1}$ as the real value will vary about the mean. Based on this a likely conclusion is that the spatial resolution of the probe could bias the measurements in the cylinder wake.

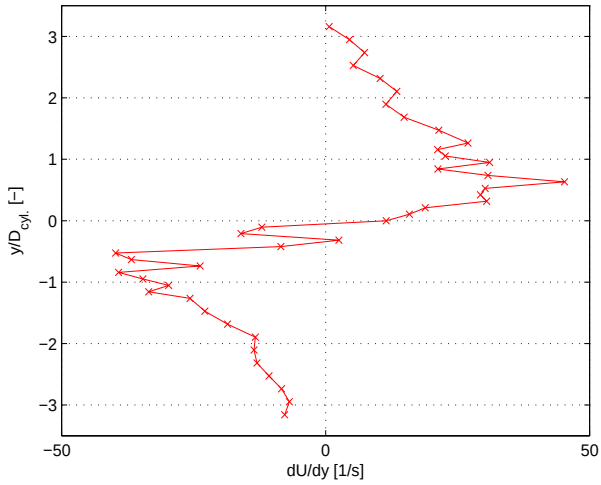

Figure 33: Gradient of U in the cylinder wake

Basing the estimate of the gradient on the streamwise velocity obtained from the hot wire is ofcourse a source of error in itself, as the gradient might bias the streamwise velocity. However the results from the pipe flow gave a relatively good fit to the logarithmic law even close to the wall, indicating that the streamwise velocity is not severly affected by the large gradient. From the pipe flow results one can conclude that all the turbulent properties are affected by the velocity gradient. In the cylinder wake the largest deviation from what was expected was found for $\overline{uw}$ and $\overline{vw}$, both shear stresses had a magnitude similar to $\overline{uv}$. It seems likely that the error is caused by the velocity gradient. Compared to litterature the normal stresses also showed some deviation, but the order of the results were correct. It does therefore seem like the turbulent shear stresses in the wake is more heavily affected by the large gradients than the turbulent normal stresses. A similar conclusion can to a certain degree also be made by studying the results from the pipe, but no decissive conclusion can be made, as the pipe data also shows scatter as a result of varying ϕ_1.

5 Future work and recommendations

Analysing the results obtained revealed that more work should have been put into aligning the probe with the flow. Designing of a holder which allowed for yawing and pitching of the probe as well as traversing could help this situation. By yawing and pitching the probe for a known velocity the results could be used to find the error in the probe alignment and correct for it in the data reduction program when analyzing the results.

If the probe is to be used in dynamic flows, such as e.g. a turbin wake it would be necesarry to investigate further how the shed vortices affect the measurements. This could be done by analysing a cylinder wake furter downstream, using both LDA and hot-wire, perhaps combined with pressure measurements on the cylinder to conditionally average the data. Going downstream the results are likely to converge at some point when the spatial resolution of the probe is sufficient compared to the gradient. The results from conditional averaging could then be used to find the gradients in the vortices etc.

If possible it would of course be beneficial to reduce the physical size of the probe.

6 Conclusion

The effective angle of the individual wires has been found from calibration in a turbulent pipe flow, the results show that the effective angle approach can be applied within a range og $\pm 20\,\mathrm{deg}$ with an uncertainty of $\pm 1\,\mathrm{deg}$ in yaw for the individual wire. The velocities matched the reference velocity obtained by pitot with a maximum relative error of 1.1%.

Measurements in the turbulent pipe flow gave a good match with the logarithmic law and the theoretical distribution of $\overline{u_x u_r}$. The normal shear stresses were in agreement with the results found by Torbergsen [9], but were found to be sensitive to probe misalignment. Outside $|y/R| > 0.8$ the probe gave bad results for shear stresses and normal stresses, due to the large gradient of the axial velocity. The radial and circumferential mean velocity was also found to be biased by the gradient, especially close to the wall for $|y/R| > 0.8$.

As long as the probe has a physical size an error must be accepted when measuring in a velocity gradient. A rough estimate of a critical gradient for the probe was set to $501/s$ based on assesment of the variation of crossstream turbulent shear stresses. The exact magnitude of the error given by the gradient is hard to find as several other sources of error also contribute to deviation from the expected result, such as probe yaw and pitch as well as inaccuratly estimated values for ϕ_1.

Measurements in the turbulent wake of the cylinder revealed the weaknesses of the measurement technique. The results give that the crosstream turbulent stresses, $\overline{uw}$ and $\overline{vw}$, are of the same order of magnitude as $\overline{uv}$. The cause is belived to be spatial resolution of the probe.

The results lead to the conclusion that the probe is capable of measuring both mean velocities and turbulent stresses with good accuracy in flows where the velocity gradient is smaller than the critcal gradient. A prerequisiteis however is that the probe is carefully aligned with the flow or that the misalignment is corrected for in the data reduction process.

Further testing is recommended to verify to what extent the probe can be used in flows where vortices are shed, e.g. tip vortices from wind turbine models.

References

[1] Are Aanesland. Utvikling av tre-komponents hetetrådsanemometri. 1998.

[2] T. Arts, H. Boerrigter, J.-M. Buclin, M. Carbonaro, G. Degrez, D. Fletcher R. Dénos, D. Olivari, M.L. Riethmuller, and R.A. Van den Braembussche. *Measurement techniques in fluid dynamics, An introduction, 2nd revised edition.* von Karman Institute for Fluid Dynamics, 2004.

[3] Brian Cantwell and Donald Coles. An experimental study of entrainment and transport in the turbulent near wake of a circular cylinder. 1983.

[4] C.H.K.Williamson. Vortex dynamics in the cylinder wake. 1996.

[5] I Lekakis. Calibration and signal interpretation for single and multiple hot-wire/hot-film probes. 1996.

[6] P.M. Ligrani and P. Bradshaw. Subminiature hot-wire sensors: development and use. 2008.

[7] L. Ong and J. Wallace. The velocity field of the turbulent very near wake of a circular cylinder. 2008.

[8] H. Tennekes and J.L. Lumley. *A first course in turbulence.* 1972.

[9] Lars Even Torbergsen. Experiments in turbulent pipe flow. 1995.

[10] Anthony J. Wheeler and Ahmad R. Ganji. *Introduction to Engineering Experimentation, Second edition.* Pearson, Prentice Hall, 2004.

[11] Frank M. White. *Fluid Meachanics, Fifth edition.* McGraw-Hill, 2001.

[12] Frank M. White. *Viscous fluid flow, third edition.* 2006.

[13] J.G. Wissink and W. Rodi. Numerical study of the near wake of a circular cylinder. 1996.

Appendices

A Data reduction program

A script (HW3Dv12.f95) has been written in Fortran to perform all calculations needed, from calibration to calculation of statistics. The program is written to be general, and easy to apply to different datasets. A textfile (filedata.txt) specifies where the input data is to be gathered and where to stor the output data. In addtion every set of angle calibration or timeseries datasets is accompanied by a file specifying transducer constants, wire temperature etc(settings.txt).

To curvefit data a Fortran program kurve-mac.f written by Per-Åge Krogstad is used, the program fits data to any equation specified and reports the result and the match between the equation and datapoints.

$$residual = \sum \left| \frac{Y(i)_{datapoint} - Y(i)_{fit}}{\frac{Y(i)_{datapoint} + Y(i)_{fit}}{2}} \right| \tag{44}$$

The datareduction was initially meant to be performed using a Fortran routine called dnsqe.f from the Slatec library. Dnsqe.f uses the more complex dnsq.f to find the zero of a system of nonlinear functions, using "a modification of the Powell hybrid method". It did however prove difficult to obtain convergence using dnsqe.f, it works for mean values but it did not find the solution in turbulent flows. As the routine was successfully used by Aanesland [1] this was suprising, and probably indicates that the routine was not applied correctly. The solution was to use Matlabs fzero function to do the same job. This was however a much slower solution, but it worked.

The script is compilated as a project in Plato to be able to combine free-format and fixed-format Fortran files, since dnsqe.f is used to solve some meanvalues in the script directly.

The original idea was that the program should be general and user friendly, the end result works as intended but is too complex. Further work would be to include more error checking, but also to dramatically simply the script.